IEEE Access
Multidisciplinary | Rapid Review | Open Access Journal

Date of publication xxxx 00, 0000, date of current version xxxx 00, 0000.

Digital Object Identifier 10.1109/ACCESS.2017.DOI

Adaptive FIT-SMC Approach for an Anthropomorphic Manipulator with Robust Exact Differentiator and Neural Network-Based Friction Compensation

KHURRAM ALI[1], SAFEER ULLAH[1], ADEEL MEHMOOD[1], HALA MOSTAFA[2], MOHAMED MAREY[3], (Senior Member, IEEE), and JAMSHED IQBAL[4], (Senior Member, IEEE)

[1]Department of Electrical and Computer Engineering, COMSATS University, Islamabad 45550, Pakistan
[2]Department of Information Technology, College of Computer and Information Sciences, Princess Nourah bint Abdulrahman University, Riyadh 84428, Saudi Arabia
[3]Smart Systems Engineering Laboratory, College of Engineering, Prince Sultan University, Riyadh 11586, Saudi Arabia
[4]Department of Computer Science and Technology, Faculty of Science and Engineering, University of Hull, HU6 7RX, UK

Corresponding author: Jamshed Iqbal (j.iqbal@hull.ac.uk).

ABSTRACT In robotic manipulators, feedback control of nonlinear systems with fast finite-time convergence is desirable. However, because of the parametric and model uncertainties, the robust control and tuning of the robotic manipulators pose many challenges related to the trajectory tracking of the robotic system. This research proposes a state-of-the-art control algorithm, which is the combination of fast integral terminal sliding mode control (FIT-SMC), robust exact differentiator (RED) observer, and feedforward neural network (FFNN) based estimator. Firstly, the dynamic model of the robotic manipulator is established for the n degrees of freedom (DoFs) system by taking into account the dynamic LuGre friction model. Then, a FIT-SMC with friction compensation-based nonlinear control has been proposed for the robotic manipulator. In addition, a RED observer is developed to get the estimates of robotic manipulator joints' velocities. Since the dynamic friction state of the LuGre friction model is unmeasurable, FFNN is established for training and estimating the friction torque. The Lyapunov method is presented to demonstrate the finite-time sliding mode enforcement and state convergence for a robotic manipulator. The proposed control approach has been simulated in the MATLAB/Simulink environment and compared with the system with no observer to characterize the control performance. Simulation results obtained with the proposed control strategy affirm its effectiveness for a multi-DoF robotic system with model-based friction compensation having an overshoot and a settling time less than 1.5% and 0.2950 seconds, respectively, for all the joints of the robotic manipulator.

INDEX TERMS robotic manipulator, robust exact differentiator, feedforward neural network, fast integral sliding mode control, LuGre friction model, autonomous articulated robotic educational platform.

I. INTRODUCTION

Researchers in academia and industry have shown a significant deal of interest in robotic manipulators in recent years due to scientific advancements and industrial needs [1]. In reality, robotic manipulators play a significant role in the industry by lowering manufacturing costs, improving accuracy, quality, and efficiency, and offering more flexibility than specialized equipment. They ought to be controlled and operated smoothly, securely, and reliably to accomplish tasks with higher throughput or productive exploration [2]. The control of robotic manipulators is a complex task because their dynamic behavior is exceptionally nonlinear, highly coupled, and time-varying. Apart from that, uncertainties in the system model, such as external disturbances, parameter uncertainty, and nonlinear frictions, constantly exist and cause the unstable performance of the robotic system [3]. In the literature, several approaches have been proposed for controlling the robotic systems, such as sliding mode control (SMC) [4] , H-infinity (H_∞) control [5], optimal control [6], PID control [7], adaptive control [8], model predictive

This article has been accepted for publication in a future issue of this journal, but has not been fully edited. Content may change prior to final publication. Citation information: DOI 10.1109/ACCESS.2021.3139041, IEEE Access

control (MPC) [9], and other nonlinear controls reported in [10]–[12].

One of the main issues impeding the fast-tracking behavior of robotic manipulators is friction, resulting in steady-state tracking inaccuracy [13]. On the other hand, nonlinear friction often causes disturbances in a control system and may even make it to unstable [14]. As a consequence, friction is an intrinsically nonlinear occurrence that is hard to predict [15]. Therefore, friction should be modeled for better control performance and efficiency. Various friction modeling techniques are available in the literature, each describing and predicting improved and more accurate friction behavior [16]. Friction models are, generally, categorized into static [17] and dynamic [18] friction models. Static models merely illustrate the direct relationship between actual velocity and friction. They ignore the friction memory effect and hysteresis resulting in inaccuracy near zero velocity. In [19], an overview of static model methods based on the Coulomb and Stribeck effects is provided. Furthermore, the dynamic models capture physical characteristics and reactions by adding up the extra state variables. To put it simply, the static and dynamic friction models vary primarily in the predicted frictional effects, computing efficiency, and implementation complexity [20]. A suitable friction model is a fundamental need for effective compensation outcomes. A dynamic model known as the LuGre model has been widely utilized because it provides a fair balance of complexity and accuracy [21] [22]. A reasonably compact formula captures the significant friction phenomena, such as Coulomb friction, viscous friction, stiction, and dynamic brittle behavior at the contact surface.

Friction is a significant element influencing the accuracy with which an actuator system places or positions itself. The feedback linearization technique may be used to compensate for known nonlinearities. In terms of friction compensation, there are two types of schemes [23]: friction model-based and friction non-model-based schemes. The concluding methodology is employed when precise friction modeling is complicated or unnecessary, such as for variable structure control [24], PD control [25], and neural network control [26]. The model-based methodology [27] may be used if the friction parameter can be accurately identified to a certain degree. For dynamic friction compensation with backstepping control in [28], a robust observer for friction and a recurrent fuzzy neural network (RFNN) were designed. The generalized Maxwell-slip (GMS) friction compensation in a two-DoF robotic manipulator utilized an online least-squares estimator to estimate the friction force in each joint [29]. A proportional derivative (PD) controller was illustrated in [30] with friction compensation. The adaptive sliding control (A-SC) algorithm with friction compensation for robotic manipulator established on fuzzy random vector function is described in [31]. The tracking control of robotic manipulator is presented in [32], the proportional derivative adaptive control approach is employed for the estimation of system dynamics, and SMC is implemented for the unknown dynamics of the robotic manipulator. A robust adaptive control technique based on fuzzy wavelet neural networks (FWNNs) dynamic structure is presented in [33]. Furthermore, using a radial basis function (RBF) neural networks technique, [34] proposed an amplitude saturation controller (ASC) that can ensure the development of exclusively saturated unidirectional attractive force for maglev vehicles on an elastic track. This paper's primary objectives and contributions are summarized as follows:

- The robot's dynamic model for the five-DoF AUTAREP robotic manipulator is built using the dynamic LuGre friction model. Under the uncertainties limited by certain positive functions, the velocity of each link is obtained using the RED observer.
- The FFNN approximates the friction torque, using the estimated velocities of joints obtained from the RED observer. Furthermore, a FIT-SMC scheme is proposed to achieve the desired trajectory tracking in finite time in the presence of uncertainties.
- Henceforth, the Lyapunov method is utilized to strengthen the robotic manipulator's stability. Results obtained from the proposed approach are illustrated in the MATLAB/Simulink environment to validate the FIT-SMC performance.

The contents in the remaining article are organized as follows: Section II presents a robotic manipulator state-space model, including the LuGre friction model. In Section III, the FIT-SMC approach is designed; RED observer, FFNN, and Lyapunov stability analysis is provided. Simulated results are provided in Section IV. Section V provides some concluding observations and remarks. Finally, Section VI presents the acknowledgment.

II. MATHEMATICAL MODELING

The effectiveness of robotic manipulators can be improved by combining high motion accuracy with high speed. Feedback robot controllers have a challenging task to accomplish this objective because they rely on the operating state without taking into account the dynamic features of the robot manipulator. In the last several years, certain model-based controllers have been created, and the performance of robot manipulators has been improved. The research in this paper has been accomplished using the Autonomous Articulated Robotic Educational Platform (AUTAREP) ED-7220C robotic manipulator as shown in Fig. 1.

A manipulator is typically comprised of a kinematic chain, and its dynamic model is influenced by various drawbacks, such as coupling among the links, low rigidity, and unknown parameters. Furthermore, nonlinear effects often induced by the actuation mechanism include dead zone and friction. Thus, a robotic manipulator's motion is greatly influenced by its dynamic modeling, which is an extremely important consideration [35]. In order to implement control algorithms, the mathematical system model is an essential requirement. It is a five-DoF articulated robotic manipulator. Each joint movement is operated by a single DC servo motor except for

This article has been accepted for publication in a future issue of this journal, but has not been fully edited. Content may change prior to final publication. Citation information: DOI 10.1109/ACCESS.2021.3139041, IEEE Access

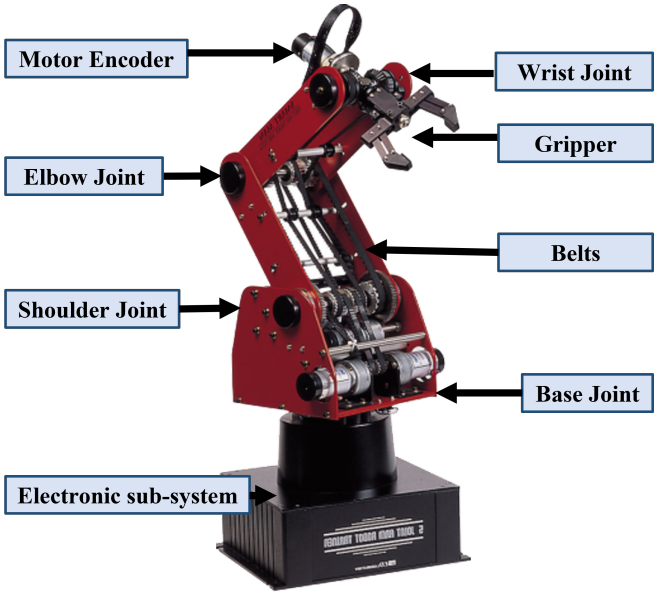

FIGURE 1. AUTAREP robotic manipulator ED-7220C.

the wrist joint, which is actuated by two motors for roll and pitch movements. The joints' location is provided through optical encoders equipped on each joint actuator axis of the robotic manipulator. Table 1 presents the robotic manipulator parameters.

TABLE 1. AUTAREP robotic manipulator parameters.

Parameters	Specifcations	Units
Links length	Base: 385	mm
	Shoulder: 220	mm
	Elbow: 220	mm
	Wrist: 155	mm
Movement speed	Approx. 100	mm/s max
Range of motion (ROM)	Base: 310	deg
	Shoulder: $+130/-35$	deg
	Eblow: ± 130	deg
	Wrist: 360 rotation, up-down $\pm$ 130	deg
Precision (position)	± 0.5	mm
Weight	33	Kg
Load capacity	1	Kg
Construction	Vertical articulated arm	
Actuator	DC servo motor (optical encoder)	
Number of joints	5 joints + gripper	

A. DYNAMIC MODEL

The forces and torques that produce robot motion are the subjects of research in dynamic modeling of the robot system. In this research, the Euler-Lagrange method is used for the n-link robotic manipulator dynamic equation [36], and it is illustrated by the following equation:

$$\tau_{r\eta} = M\left(r_\eta\right)\ddot{r}_\eta + C_F\left(r_\eta, \dot{r}_\eta\right)\dot{r}_\eta + G\left(r_\eta\right) + T_F\left(\dot{r}_\eta\right), \quad (1)$$

where for n joints, $M(r_\eta) \in \mathbb{R}^{n\times n}$ is the mass matrix, $G(r_\eta) \in \mathbb{R}^{n\times 1}$ describe the gravitational matrix, $C_F(r_\eta) \in \mathbb{R}^{n\times n}$ represents the centripetal and Coriolis forces, $T_F(\dot{r}_\eta) \in \mathbb{R}^{n\times 1}$ represents friction torques, and total torque of robotic manipulator joints is denoted by $\tau_{r\eta}$.

The characteristics of the robotic manipulator dynamics in Eq. (1) are as follows.

Property I

The matrix of inertia $M(r_\eta)$ is symmetric, is positive definite, and satisfies the condition given in the following equation [37]:

$$\Omega_1 I_\eta \leq M(r_\eta) \leq \Omega_2 I_\eta, \quad (2)$$

where Ω_1 and Ω_1 are constants having positive value and I_η is the identity matrix.

Property II

The $C_F(r_i)$ centrifugal and Coriolis matrix in a dynamic robotic manipulator model justifies the following equation [37]:

$$\|C_F(r_\eta, \dot{r}_\eta)\| \leq \Omega_3 \|r_\eta\|, \qquad \forall r_\eta, \dot{r_\eta} \in \mathbb{R}^n, \quad (3)$$

where Ω_3 is the positive constant and $\|(.)\|$ is the Euclidean norm.

Property III

The term G in Eq. (1) is defined as a gravitational quantity [38] bounded as

$$\|G\| \leq g_b \quad \forall r_\eta \in \mathbb{R}^n, \quad (4)$$

where g_b is defined as a positive function of r_η.

Property IV

$N(r_\eta, \dot{r}_\eta) = \dot{M}(r_\eta) - 2C_F(r_\eta, \dot{r}_\eta)$ is a skew symmetric [39]; that is, the components η_{jk} of N satisfy $\eta_{jk} = -\eta_{kj}$ and assure the following equation [38]:

$$x^T \left[\dot{M}(r_\eta) - 2C_F(r_\eta, \dot{r}_\eta)\right] x = 0, \quad \forall x \in \mathbb{R}^n. \quad (5)$$

B. DYANMIC LUGRE FRICTION MODEL

Friction is also a significant factor in the performance of control systems. Friction reduces the precision of positioning and pointing systems, and it can also cause instabilities in the system. Friction compensation can help mitigate the negative impact of friction to a certain extent. It is beneficial to have simple models of friction that capture the essential properties of friction for use in control applications. The LuGre friction

This article has been accepted for publication in a future issue of this journal, but has not been fully edited. Content may change prior to final publication. Citation information: DOI 10.1109/ACCESS.2021.3139041, IEEE Access

model [40], a nonlinear dynamic friction model widely used in mechanical and servo systems, will be used to formulate the dynamic friction $T_{F\eta}$ in this subsection [41]. The LuGre model is defined as in Eq. (6) and Eq. (7) and Table 2 demonstrates the LuGre friction model parameters.

$$\frac{dz_F}{dt} = \omega - \sigma_0 \frac{|\ \omega\ |}{g\ (\omega)}\ z_F, \tag{6}$$

$$T_{F\eta} = \sigma_0\ z_F + \sigma_1 \dot{z}_F + \ f(\omega), \tag{7}$$

$$T_{F\eta} = \sigma_0\ z_F + \sigma_1 \dot{z}_F + \ \sigma_2 \omega, \tag{8}$$

where $T_{F\eta}$ is the predicted friction torque, its internal state is described by z_F, ω is the velocity between the two surfaces in contact, the function ω that changes with velocity is illustrated in Eq. (9), and σ_1 and σ_0 are coefficients for bristles.

$$g_\eta(\omega) = \tau_{c\eta} + (\tau_{s\eta} - \tau_{c\eta}) \exp^{-\ (|\omega/\omega_s|)}, \tag{9}$$

where $\tau_{c\eta}$ represents the Coulomb friction torque and $\tau_{s\eta}$ describes the stiction torque. The ω_s factor determines precisely how $g_\eta(\omega)$ reaches the Coulomb torque $\tau_{c\eta}$ immediately.

TABLE 2. Parameters of the LuGre friction model.

Parameter	Description	Value	Unit
ω_s	Velocity	$6.109.10^{-2}$	rad/sec
σ_2	Viscous friction coefficients	1.819	Nm.sec/rad
σ_1	Damping coefficient	45.2	Nm.sec/rad
σ_0	Stiffness coefficient	2750	Nm/rad
$\tau_{s\eta}$	Static friction torque	8.875	Nm
$\tau_{c\eta}$	Coulomb friction torque	6.975275	Nm

III. CONTROL DESIGN AND MATHEMATICAL PRELIMINARIES

Due to nonlinearities and uncertainties in robotic dynamical models, adaptive control has been acknowledged as a viable method for mechanical robotic controller design. An innovative stable finite-time controller design for five-DoF robotic manipulators is given in Fig. 2 that uses FIT-SMC-based law, a variable-gain RED, and FFNN to achieve the ultimate aim.

The AUTAREP robotic manipulator system is presented in Eq. (10) as a state-space model, where $r_{1\eta}$ is the state variable of position, $r_{2\eta}$ is the velocity state variable, and r_{z_η} is the friction state of the dynamic LuGre friction model.

$$\left.\begin{aligned} \dot{r}_{1\eta} &= r_{2\eta} \\ \dot{r}_{2\eta} &= M^{-1}\tau_r - M^{-1}(C_F r_{2\eta} + G r_{1\eta} + \sigma_0 r_{z_\eta} \\ &\quad + \sigma_2 r_{2\eta} + \sigma_1 \dot{r}_{z_\eta}) \\ \dot{r}_{z_\eta} &= r_{2\eta} - \sigma_0 \frac{|r_{2\eta}|}{g\ (r_{2\eta})} r_{z_\eta} \end{aligned}\right\}, \tag{10}$$

where $\eta = b(base/waist), s(shoulder), e(elbow), w(wrist)$. The control law has three main phases. First, a robust FIT-SMC is developed to guarantee and ensure the global boundness of the robot manipulator system in the occurrence of uncertainty and disturbance. Secondly, the velocities of the system are estimated by utilizing variable-gain RED observer. In the third phase, FFNN is applied to estimate friction torque as the friction in the robotic manipulator model is not measurable. In the recent literature, a fast TSMC technique has been extensively used to achieve speedy finite-time stability.

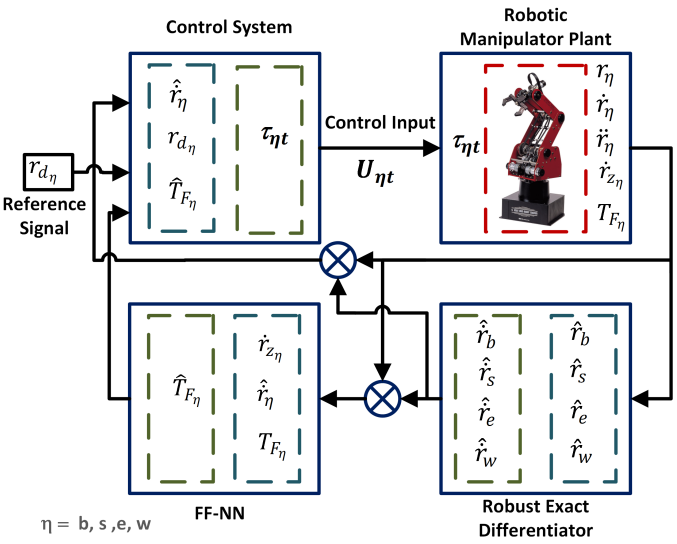

FIGURE 2. Block diagram.

A. VARIABLE-GAIN ROBUST EXACT DIFFERENTIATOR

A second-order nonlinear dynamics of the robotic manipulator may be expressed as follows in order to demonstrate the differentiator design:

$$\left.\begin{aligned} \dot{\bar{r}}_{1\eta} &= \bar{r}_{2\eta} \\ \dot{\bar{r}}_{2\eta} &= J_{\bar{r}_\eta}(t, \bar{r}_\eta) + K_{\bar{r}_\eta}(t, \bar{r}_\eta) U_{\bar{r}_\eta}(t, \bar{r}_\eta) \end{aligned}\right\}, \tag{11}$$

where $\bar{r}_\eta = [\bar{r}_{1\eta}, \bar{r}_{2\eta}]$ and $\eta = b, s, e, w$.

$$\psi_{1\eta} = \hat{\bar{r}}_{1\eta} - \bar{r}_{1\eta}, \tag{12}$$

$$\psi_{2\eta} = \hat{\dot{\bar{r}}}_{2\eta} - \dot{\bar{r}}_{1\eta}. \tag{13}$$

The RED observer design will provide the estimated/predicted derivatives for the available positions. In other terms, every $r_{1\eta}$ will provide $r_{2\eta}$ estimations. Moreover, the dynamics of tracking error may be described as follows:

$$\left.\begin{aligned} \dot{\psi}_{1\eta} &= -\Lambda_{i1}(t, \bar{r}_i)|\psi_{1\eta}|^{1/2} sign(\psi_{1\eta}) + \psi_{2\eta}, \\ \dot{\psi}_{2\eta} &= -\frac{\Lambda_{i2}(t, \bar{r}_i)}{2} sign(\psi_{1\eta}) - \ddot{r}_{1\eta}. \end{aligned}\right\} \tag{14}$$

To construct the control algorithm, most controllers need all state variables. In reality, however, all state variables are unavailable for measurement for various economic and technological reasons. The high-frequency gain is boosted

This article has been accepted for publication in a future issue of this journal, but has not been fully edited. Content may change prior to final publication. Citation information: DOI 10.1109/ACCESS.2021.3139041, IEEE Access

by a differentiator (classical). The controller design requires the whole state to be accessible; however, in this study, only the measurements of position states are considered to be available. As a result, to estimate its velocities, a smooth differentiator is used as an observer. The proposed differentiator has a unique feature that reduces high-frequency chattering compared to the conventional sliding mode-based differentiators. The globally converging RED is taken into account.

$$\dot{\hat{\bar{r}}}_{1\eta} = -\gamma_{1\eta}(t,\bar{r}_\eta)|\psi_{1\eta}|^{1/2} sign\psi_{1\eta} + \hat{\bar{r}}_{i2}, \tag{15}$$

$$\dot{\hat{\bar{r}}}_{2\eta} = -\frac{\gamma_{2\eta}(t,\bar{r}_\eta)}{2} sign\psi_{1\eta}, \tag{16}$$

where $\gamma_{1\eta}$ and $\gamma_{2\eta}$ are the variable gains of RED observer expressed in Eq. (15) and Eq. (16), respectively:

$$\gamma_{1\eta}(t,\bar{r}_\eta) = \chi_i + \frac{1}{\beta_i}\left[\frac{V_\eta^2(t,\bar{r}_\eta)}{2\epsilon_i} + 2\epsilon_i(\beta_i + 4\epsilon_i^2) + 4\epsilon_i V_\eta(t,\bar{r}_\eta)\right], \tag{17}$$

$$\gamma_{2\eta}(t,\bar{r}_\eta) = 2\epsilon_i\gamma_{1\eta}(t,\bar{r}_\eta) + \beta_i + 4\epsilon_i^2, \tag{18}$$

where $i = 1,2,3,4$, $\eta = b,s,e,w$ and the arbitrary positive constants are χ_i, ϵ_i, β_i. It is worth noting that the error dynamics are globally converged to zero in limited time with the aid of this velocity observer. Now, the previously mentioned robust global convergence differentiator can be used to estimate the derivatives of the AUTAREP robotic manipulator system.

For the waist (base) joint,

$$\left.\begin{aligned}
\dot{\hat{r}}_{1b} &= -\gamma_{1b}|\hat{r}_{1b} - r_{1b}|^{1/2} sign(\hat{r}_{1b} - r_{1b}) + \hat{r}_{1b},\\
\dot{\hat{r}}_{2b} &= -\frac{\gamma_{2b}}{2} sign(\hat{r}_{1b} - r_{1b})\\
\gamma_{1b} &= \delta_1 + \frac{1}{\beta_1}\left(\frac{V_1^2}{2\epsilon_1} + 2\epsilon_1(\beta_1 + 4\epsilon_1^2) + 4\epsilon_1 V_1\right),\\
\gamma_{2b} &= 2\epsilon_1\gamma_{1b} + \beta_1 + 4\epsilon_1^2
\end{aligned}\right\}. \tag{19}$$

For the shoulder joint,

$$\left.\begin{aligned}
\dot{\hat{r}}_{1s} &= -\gamma_{1s}|\hat{r}_{1s} - r_{1s}|^{1/2} sign(\hat{r}_{1s} - r_{1s}) + \hat{r}_{2s},\\
\dot{\hat{r}}_{2s} &= -\frac{\gamma_{2s}}{2} sign(\hat{r}_{1s} - r_{1s})\\
\gamma_{1s} &= \delta_2 + \frac{1}{\beta_2}\left(\frac{V_2^2}{2\epsilon_2} + 2\epsilon_2(\beta_2 + 4\epsilon_2^2) + 4\epsilon_2 V_2\right),\\
\gamma_{2s} &= 2\epsilon_2\gamma_{1s} + \beta_2 + 4\epsilon_2^2
\end{aligned}\right\}. \tag{20}$$

For the elbow joint,

$$\left.\begin{aligned}
\dot{\hat{r}}_{1e} &= -\gamma_{1e}|\hat{r}_{1e} - r_{1e}|^{1/2} sign(\hat{r}_{e1} - r_{1e}) + \hat{r}_{2e},\\
\dot{\hat{r}}_{2e} &= -\frac{\gamma_{2e}}{2} sign(\hat{r}_{1e} - r_{1e})\\
\gamma_{1e} &= \delta_3 + \frac{1}{\beta_3}\left(\frac{V_3^2}{2\epsilon_3} + 2\epsilon_3(\beta_3 + 4\epsilon_3^2) + 4\epsilon_3 V_3\right),\\
\gamma_{2e} &= 2\epsilon_3\gamma_{1e} + \beta_3 + 4\epsilon_3^2
\end{aligned}\right\}. \tag{21}$$

For the wrist joint,

$$\left.\begin{aligned}
\dot{\hat{r}}_{1w} &= -\gamma_{1w}|\hat{r}_{1w} - r_{1w}|^{1/2} sign(\hat{r}_{1w} - r_{1w}) + \hat{r}_{2w},\\
\dot{\hat{r}}_{2w} &= -\frac{\gamma_{2w}}{2} sign(\hat{r}_{1w} - r_{1w})\\
\gamma_{1w} &= \delta_4 + \frac{1}{\beta_4}\left(\frac{V_4^2}{2\epsilon_4} + 2\epsilon_4(\beta_4 + 4\epsilon_4^2) + 4\epsilon_4 V_4\right),\\
\gamma_{2w} &= 2\epsilon_4\gamma_{1w} + \beta_4 + 4\epsilon_4^2
\end{aligned}\right\}. \tag{22}$$

B. NEURAL NETWORK-BASED APPROXIMATION

In recent years, controllers based on neural networks (NN) have gained significant interest. The controller uses neural networks' capabilities to learn nonlinear functions and handle specific problems that need large parallel computing. This subsection discusses how to approximate friction torque $(T_{F\eta})$ using a FFNN and it is presented in Fig.3. The network's information flows exclusively in the forward direction. It starts from the level of the input layer and later flows to the level of hidden layers, if they are any. Finally, it concludes at the output layer. The output of feedforward networks is entirely dependent on the network input (and, in some instances, the output is constant while the network input is fixed).

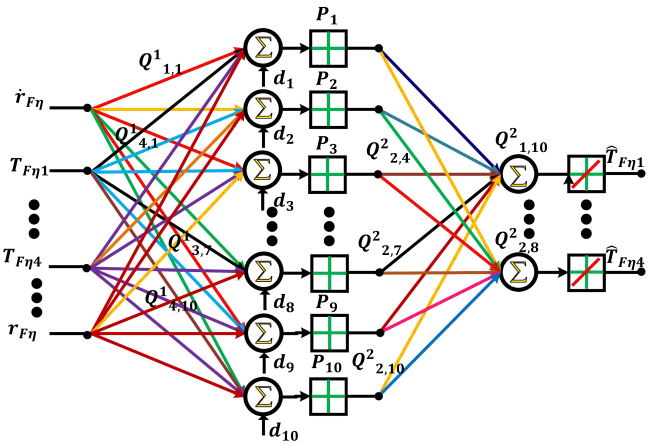

FIGURE 3. FFNN for robotic manipulator.

The approximation function under consideration is a three-layer feedforward neural network (TLFFNN). The TLFFNN consists of one input layer with one hidden layer and one output layer. The hidden layer of TLFFNN has artificial neurons, N=10. The artificial NN is primarily trained and guided by mapping the input data to the output data. As soon as the system has been trained, the estimated model functions will adapt autonomously and then provide the desired output under running conditions based on the training data provided by the user. Optimization techniques are used in the training of the artificial NN. It is worth noting that the friction states $r_{z\eta}$ and $\dot{r}_{z\eta}$ of the robotic manipulator and the estimated velocity of the joints obtained from robust

This article has been accepted for publication in a future issue of this journal, but has not been fully edited. Content may change prior to final publication. Citation information: DOI 10.1109/ACCESS.2021.3139041, IEEE Access

exact differentiator functioned as inputs of TLFFNN. $T_{F\eta}$ is considered a network output. Consider $T_{F\eta} = J_r$:

$$\left.\begin{aligned} P_N &= \mathcal{N}_N^1\Big(\sum_{n=1}^{N} Q_{N,n}^1 X + d_N^1\Big) \\ &= \mathcal{N}_N^1\Big(\mathbf{Q}_N^{1^T}\mathbf{X}_n + d_N^1\Big), \\ \hat{J}_r &= \mathcal{N}_m^2\Big(\sum_{N=1}^{m} \hat{Q}_{J_r,N}^2 P_N\Big) \\ &= \hat{\mathbf{Q}}_{J_r}^{2^T}\mathbf{P}_N \end{aligned}\right\}, \tag{23}$$

where $n = 3$ and $m = 1$ denote the number of network inputs and outputs for a single joint of robotic manipulator, respectively (for all joints, $n = 12$ and $m = 4$). The hidden layer of neurons is $N = 10$ and $M = 4$ is the number of output layer neurons.

The tan-sigmoid $\mathcal{N}_N^1 \in \mathbb{R}^n \to \mathbb{R}^N$ and pure linear activation $\mathcal{N}_M^2 \in \mathbb{R}^M \to \mathbb{R}^m$ are functions of the hidden layer neuron and output layer neuron, respectively. $b_N^1 \in \mathbb{R}^n$ demonstrate the network bias that are utilized to improve learning speed during network training. The input vector is described as $X = [r_{z\eta} \quad \dot{r}_{z\eta} \quad \dot{r}_{1\eta}] \in \mathbb{R}^n$. $\hat{T}_{F\eta}$ is the desired target output. $Q_N^1 \in \mathbb{R}^n$ and $Q_{J_r}^2$ are the hidden layer and output layers weights vector, respectively. The suggested NN's output algorithm is as follows:

$$J_r = \mathbf{Q}_{J_r}^{2^T}\mathbf{P} + e_J, \tag{24}$$

where e_J describes the network approximation error.

$$\begin{aligned} \tilde{J}_r &= \hat{J}_r - J_r = \tilde{T}_{F\eta} \\ &= \tilde{\mathbf{Q}}_{J_r}^{2^T}\mathbf{P} - e_J \end{aligned} \tag{25}$$

$$\left.\begin{aligned} \tilde{\mathbf{Q}}_{J_r}^2 &= \hat{\mathbf{Q}}_{J_r}^2 - \mathbf{Q}_{J_r}^2, \\ \dot{\tilde{\mathbf{Q}}}_{J_r}^2 &= \dot{\hat{\mathbf{Q}}}_{J_r}^2 \end{aligned}\right\}. \tag{26}$$

C. FIT-SMC SCHEME

The difference between the expected and reference trajectories in the controller that generates the control inputs is utilized as a performance benchmark. The speed of the different motors fluctuates and varies as the control inputs are supplied to the actuator. As an outcome, the underlying system's anticipated motion is accomplished. The reference tracking errors expressed for the said purpose are given in the following equation:

$$\begin{aligned} e_\eta &= r_{1\eta} - r_{d\eta}, \\ \dot{e}_\eta &= \dot{r}_{1\eta} - \dot{r}_{d\eta}, \\ \ddot{e}_\eta &= \ddot{r}_{1\eta} - \ddot{r}_{d\eta}. \end{aligned} \tag{27}$$

In contrast to the conventional SMC-based designs, TSMC has superior speedy and finite-time convergence characteristics, which improves high-precision control performance by increasing the convergence rate towards an equilibrium point. Consider the sliding surface manifold design as described in the following equation to accomplish the primary control objectives:

$$\delta_\eta = \dot{e}_\eta + \alpha_\eta e_\eta + \beta_\eta \int_0^t |e_\eta|^{\gamma_\eta} sign(e_\eta) dt, \tag{28}$$

where $\delta_\eta \in \mathbb{R}^n$, α_η, $\beta_\eta > 0$, and $0 < \gamma_\eta < 1$ is the positive number. Henceforth, the time derivative of $\delta_\eta(t)$ is used to retain the system on the integral terminal sliding surface $\delta_\eta(t) = 0$. The time derivative of Eq. (28) is determined as follows:

$$\dot{\delta}_\eta = \ddot{e}_\eta + \alpha_\eta \dot{e}_\eta + \beta_\eta |\dot{e}_\eta|^{\gamma_\eta} sign(e_\eta). \tag{29}$$

The objective is accomplished in SMC by setting $\dot{\delta}_\eta = 0$. Using this value as a substitute in Eq. (29),

$$0 = \ddot{e}_\eta + \alpha_\eta \dot{e}_\eta + \beta_\eta |\dot{e}_\eta|^{\gamma_\eta} sign(e_\eta). \tag{30}$$

Substituting the values of error dynamics from Eq. (27) into Eq. (30),

$$\begin{aligned} 0 =& \dot{r}_{2\eta} - \ddot{r}_{d\eta} + \alpha_\eta(\dot{r}_{1\eta} - \dot{r}_{d\eta}) + \beta_\eta |\dot{r}_{1\eta} - \dot{r}_{d\eta}|^{\gamma_\eta} \\ & sign(r_{1\eta} - r_{d\eta}), \end{aligned} \tag{31}$$

$$\begin{aligned} \dot{r}_{2\eta} =& \ddot{r}_{d\eta} - \alpha_\eta(\dot{r}_{1\eta} - \dot{r}_{d\eta}) - \beta_\eta |\dot{r}_{1\eta} - \dot{r}_{d\eta}|^{\gamma_\eta} \\ & sign(r_{1\eta} - r_{d\eta}). \end{aligned} \tag{32}$$

Replace the value of $\dot{r}_{2\eta}$ in Eq. (32) from Eq. (10). Therefore, Eq. (31) after considering TLFFNN can be written as follows:

$$\begin{aligned} 0 =& M^{-1}\Big[\tau_\eta - (C_F r_{2\eta} + G r_{1\eta} + \hat{T}_{F_\eta})\Big] \\ & - \ddot{r}_{d\eta} + \alpha_\eta(\dot{r}_{1\eta} - \dot{r}_{d\eta}) + \beta_\eta |\dot{r}_{1\eta} - \dot{r}_{d\eta}|^{\gamma_\eta} \\ & sign(r_{1\eta} - r_{d\eta}). \end{aligned} \tag{33}$$

Solving Eq. (33) for τ_η, we get

$$\begin{aligned} \tau_\eta =& M\Big[\ddot{r}_{d\eta} - \alpha_\eta(r_{1\eta} - \dot{r}_{d\eta}) - \beta_\eta |r_{1\eta} - \dot{r}_{d\eta}|^{\gamma_\eta} + \\ & sign(r_{1\eta} - r_{d\eta})\Big] + C_F r_{2\eta} + G r_{1\eta} + \hat{T}_{F_\eta} \end{aligned} \tag{34}$$

The SMC law's control input is divided into two components. The equivalent control legislation ($\tau_{\eta eq}$) is the first component, and it is a continuous term. The signum function is used in the second half of the discontinuous control legislation ($\tau_{\eta dis}$). The sliding phase drive system guarantees slide to equilibrium, while the reaching phase drive system maintains a steady manifold. Consider the robotic manipulator system's overall control law ($\tau_{\eta t}$) as follows:

$$\tau_{\eta t} = \tau_{\eta_{dis}} + \tau_{\eta_{eq}}. \tag{35}$$

The discontinuous function $\tau_{\eta dis}$ is defined in the following equation to compensate for the dynamic model uncertainties.

$$\tau_{\eta dis} = -\Upsilon_{1\eta}\delta_\eta - \Upsilon_{2\eta} sign(\delta_\eta). \tag{36}$$

This article has been accepted for publication in a future issue of this journal, but has not been fully edited. Content may change prior to final publication. Citation information: DOI 10.1109/ACCESS.2021.3139041, IEEE Access

The equivalent control input $\tau_{\eta eq}$ can be described as in the following equation:

$$\begin{aligned}\tau_{\eta eq} =& M\Big[\ddot{r}_{d\eta} - \alpha_\eta(r_{1\eta} - \dot{r}_{d\eta}) - \beta_\eta|r_{1\eta} - \dot{r}_{d\eta}|^{\gamma_\eta} \\ & sign(r_{1\eta} - r_{d\eta})\Big] + C_F r_{2\eta} + G r_{1\eta} + \hat{T}_{F_\eta}.\end{aligned} \tag{37}$$

By invoking the values from Eq. (36) and Eq. (37) into Eq. (35), the total control effort $\tau_{\eta t}$ of robotic manipulator system is given by the following:

$$\begin{aligned}\tau_{\eta t} =& M\Big[\ddot{r}_{d\eta} - \alpha_\eta(r_{1\eta} - \dot{r}_{d\eta}) - \beta_\eta|r_{1\eta} - \dot{r}_{d\eta}|^{\gamma_\eta} \\ & sign(r_{1\eta} - r_{d\eta})\Big] + C_F r_{2\eta} + G r_{1\eta} + \hat{T}_{F_\eta} \\ & - \Upsilon_{1\eta}\delta_\eta - \Upsilon_{2\eta} sign(\delta_\eta),\end{aligned} \tag{38}$$

where $\Upsilon_{1\eta}$ and $\Upsilon_{2\eta}$ are constants with positive value. The control input $\tau_{\eta t}$ will be used to execute the tracking task for robotic manipulator joints.

The following theorem is presented to demonstrate sliding mode enforcement and tracking errors convergence in finite time.

Theorem 1. *Consider the robotic manipulator dynamics described by Eq.* (10)*. In the presence of matched uncertainties, the proposed Eq.* (28)*, the reaching law Eq.* (36)*, and the robust control law Eq.* (38) *provide finite-time enforcement of the sliding mode. Furthermore, the tracking errors converge to the origin in a finite amount of time.*

Proof. In order to prove the above statement theorem, the Lyapunov function time derivative is given by function L_r, along the dynamics Eq. (10), one gets

$$L_r = \frac{1}{2}\delta_\eta^2, \tag{39}$$

$$\dot{L}_r = \delta_\eta \dot{\delta}_\eta, \tag{40}$$

$$\begin{aligned}\dot{L}_r =& \delta_\eta\Big[M^{-1}(\tau_{\eta t} - (C_F r_{2\eta} + G r_{1\eta} + \hat{T}_{F\eta})) \\ & - \ddot{r}_{d\eta} + \alpha_\eta(\dot{r}_{1\eta} - \dot{r}_{d\eta}) + \beta_\eta|\dot{r}_{1\eta} - \dot{r}_{d\eta}|^{\gamma_\eta} \\ & sign(r_{1\eta} - r_{d\eta})\Big].\end{aligned} \tag{41}$$

Substituting Eq. (38) in Eq. (41) and then re-arranging it, one has

$$\begin{aligned}\dot{L}_r =& \delta_\eta\left(-\Upsilon_{1\eta}\delta_\eta - \Upsilon_{2\eta} sign(\delta_\eta)\right) \\ \leq& -\Upsilon_{1\eta}\delta_\eta^2 - \Upsilon_{2\eta}|\delta_\eta|\end{aligned}, \tag{42}$$

$$\dot{L}_r + 2\Upsilon_{1\eta} L_r + \sqrt{2L_r}\Upsilon_{2\eta} \leq 0, \tag{43}$$

where $\bar{\Upsilon}_{1\eta} = 2\Upsilon_{1\eta}$, $\bar{\Upsilon}_{2\eta} = \sqrt{2}\Upsilon_{2\eta}$,

$$\dot{L}_r + \bar{\Upsilon}_{1\eta} L_r + \bar{\Upsilon}_{2\eta}\sqrt{L_r} \leq 0. \tag{44}$$

The numerical expression of the settling time is derived from Eq. (44) in the following form:

$$T_S \leq \frac{1}{2\bar{\Upsilon}_{1\eta}} \ln\left(\frac{\bar{\Upsilon}_{1\eta}\sqrt{L_r}\,(s_z\,(0)) + \bar{\Upsilon}_{2\eta}}{\bar{\Upsilon}_{2\eta}}\right). \tag{45}$$

The finite-time FIT-SMC function defined in Eq. (28) is ensured by the differential inequality in Eq. (44) with sliding mode convergence time in Eq. (45). Now, it is abundantly obvious that $\delta_\eta = 0$ is obtained by ensuring sliding modes along Eq. (28). To put that into perspective, when δ_η approaches zero, one must deal with

$$\ddot{e}_\eta + \alpha_\eta \dot{e}_\eta + \beta_\eta|\dot{e}_\eta|^{\gamma_\eta} sign(e_\eta) = 0. \tag{46}$$

The second-order differential equation is finite-time stable in δ_η; i.e., $\delta_\eta \longrightarrow 0$ in finite time. It is worth noting that the estimation of frictional torque is done using FFNNs. It is appropriate to address neural networks in the following subsection at this stage.

D. STABILITY ANALYSIS WITH LYAPUNOV FUNCTION

For stability analysis, the enhanced Lyapunov function is described as follows:

$$V = \frac{1}{2}\delta_\eta^2 + \frac{1}{2\zeta_1}\tilde{\mathbf{Q}}_{J_r}^{2^T}\tilde{\mathbf{Q}}_{J_r}^2. \tag{47}$$

The Lyapunov candidate function derivative is computed as follows:

$$\dot{V} = \delta_\eta\dot{\delta}_\eta + \frac{1}{\zeta_1}\tilde{\mathbf{Q}}_{J_r}^{2^T}\dot{\hat{\mathbf{Q}}}_{J_r}^2. \tag{48}$$

By substituting the values of $\dot{\delta}_\eta$ from Eq. (33),

$$\begin{aligned}\dot{V} =& \delta_\eta\Big[\dot{r}_{2\eta} - \ddot{r}_{d\eta} + \alpha_\eta(\dot{r}_{1\eta} - \dot{r}_{d\eta}) + \beta_\eta|\dot{r}_{1\eta} - \dot{r}_{d\eta}|^{\gamma_\eta} \\ & sign(r_{1\eta} - r_{d\eta})\Big] + \frac{1}{\zeta_1}\tilde{\mathbf{Q}}_{J_r}^{2^T}\dot{\hat{\mathbf{Q}}}_{J_r}^2.\end{aligned} \tag{49}$$

By replacing the value of $\dot{r}_{2\eta}$ with estimated friction torque $T_{z\eta}$, Eq. (49) after TLFFNN is

$$\begin{aligned}\dot{V} =& \delta_\eta\Big[M^{-1}(\tau_{\eta t} - (C_F r_{2\eta} + G r_{1\eta} + \hat{T}_{F\eta})) \\ & - \ddot{r}_{d\eta} + \alpha_\eta(\dot{r}_{1\eta} - \dot{r}_{d\eta}) + \beta_\eta|\dot{r}_{1\eta} - \dot{r}_{d\eta}|^{\gamma_\eta} \\ & sign(r_{1\eta} - r_{d\eta})\Big] + \frac{1}{\zeta_1}\tilde{\mathbf{Q}}_{J_r}^{2^T}\dot{\hat{\mathbf{Q}}}_{J_r}^2.\end{aligned} \tag{50}$$

The control input is built accordingly after evaluation of TLFFNN is demonstrated as follows:

$$\begin{aligned}\tau_{\eta t} =& M\Big[\ddot{r}_{d\eta} - \alpha_\eta(r_{1\eta} - \dot{r}_{d\eta}) - \beta_\eta|r_{1\eta} - \dot{r}_{d\eta}|^{\gamma_\eta} \\ & sign(r_{1\eta} - r_{d\eta})\Big] + C_F r_{2\eta} + G r_{1\eta} + \hat{T}_{F\eta} - \\ & - \Upsilon_{1\eta}\delta_\eta - \Upsilon_{2\eta} sign(\delta_\eta).\end{aligned} \tag{51}$$

By inserting the value of control input from Eq. (51), we get

$$\begin{aligned}\dot{V} =& \delta_\eta\Big[-\Upsilon_{1\eta}\delta_\eta - \Upsilon_{2\eta} sign(\delta_\eta) - C_F r_{2\eta} - G r_{1\eta} - \hat{T}_{F\eta} \\ & - M(\ddot{r}_{d\eta} - \alpha_\eta(\dot{r}_{1\eta} - \dot{r}_{d\eta}) - \\ & \beta_\eta|\dot{r}_{1\eta} + \dot{r}_{d\eta}|^{\gamma_\eta} sign(r_{1\eta} - r_{d\eta}))\Big] + \frac{1}{\zeta_1}\tilde{\mathbf{Q}}_{J_r}^{2^T}\dot{\hat{\mathbf{Q}}}_{J_r}^2.\end{aligned} \tag{52}$$

This article has been accepted for publication in a future issue of this journal, but has not been fully edited. Content may change prior to final publication. Citation information: DOI 10.1109/ACCESS.2021.3139041, IEEE Access

By solving Eq. (52) and taking Eq. (23) and Eq. (24) into consideration, we get

$$\dot{V} = \delta_\eta \left(- \Upsilon_1 \delta_\eta - \Upsilon_2 sign(\delta_\eta) - \tilde{\mathbf{Q}}_{J_r}^{2^T} \mathbf{P} + e_J \right) + \frac{1}{\zeta_1} \tilde{\mathbf{Q}}_{J_r}^{2^T} \dot{\hat{\mathbf{Q}}}_{J_r}^2, \tag{53}$$

$$\dot{V} = - \Upsilon_1 {\delta_\eta}^2 - \Upsilon_2 \delta_\eta sign(\delta_\eta) + \delta_\eta e_J - \delta_\eta \tilde{\mathbf{Q}}_{J_r}^{2^T} \mathbf{P} + \frac{1}{\zeta_1} \tilde{\mathbf{Q}}_{J_r}^{2^T} \dot{\hat{\mathbf{Q}}}_{J_r}^2, \tag{54}$$

$$\dot{V} = - \Upsilon_1 {\delta_\eta}^2 - \Upsilon_2 \delta_\eta sign(\delta_\eta) + \delta_\eta (e_J) - \tilde{\mathbf{Q}}_{J_r}^{2^T} \left(\delta_\eta \mathbf{P} - \frac{1}{\zeta_1} \dot{\hat{\mathbf{Q}}}_{J_r}^2 \right). \tag{55}$$

The predicted weight selected from the above Eq. (55) is as follows:

$$\dot{\hat{\mathbf{Q}}}_{J_r}^2 = \zeta_1 \mathbf{P} \delta_\eta \tag{56}$$

.

The e_J elements are assumed to be norm bounded by a constant $\Gamma_\alpha \in \mathbb{R}^n$ having positive value. Therefore, Eq. (56) can be written as follows:

$$\dot{V} = - \Upsilon_1 \delta_\eta^2 - \Upsilon_2 \delta_\eta sign(\delta_\eta) + \delta_\eta \Gamma_\alpha, \tag{57}$$

$$\dot{V} \leq -\Upsilon_1 \delta_\eta^2 - \left[\Upsilon_2 - |\Gamma_\alpha| \right] |\delta_\eta|, \tag{58}$$

where Υ_1 is a constant with a positive value and if the gain of controller Υ_2 is selected in such a manner that $\Upsilon_2 > |\Gamma_\alpha|$, then Eq. (58) can be written as Eq. (59). Therefore, Eq. (59) would be negatively semidefinite:

$$\dot{V} \leq - \Upsilon_1 \delta_\eta^2 - \Delta |\delta_\eta|, \tag{59}$$

where Δ in Eq. (59) is defined as $\Delta = \min(\Upsilon_2 - \Delta,\ \Upsilon_2 + \Delta)$. As approximation error e_J based on NN has a minimum value, the state of the system achieves an equilibrium point in finite duration.

IV. SIMULATION RESULTS AND DISCUSSION

The proposed control technique has been simulated in MATLAB/Simulink for AUTAREP five-DoF robotic manipulator. A step signal is employed to the controller for the trajectory control of the AUTAREP robotic manipulator. Fig. 4 demonstrates the trajectory control of robotic manipulator joints with desired step input signal. The suggested control methodology assures the closed-loop equilibrium convergence in a finite time and has a fast convergence rate. The conventional sliding mode's asymptotic convergence of states is overcome and it a better convergence feature than regular SMC.

The settling time of AUTAREP robotic manipulator joints after implementing the control algorithm is approximately between 0.2 secs and 0.3 secs. Similarly, the percentage overshoot of the AUTAREP robotic manipulator joints is below 1.5%. Table 3 presents the AUTAREP robot manipulator joints' performance parameters such as overshoot, settling time, and rise time

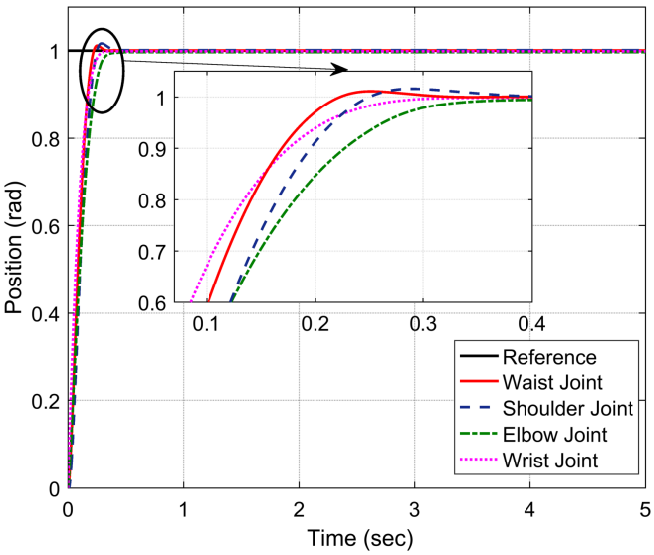

FIGURE 4. Step response of robotic manipulator joints.

The control input torque ($\tau_{\eta t}$) of the robotic manipulator is illustrated in Fig. 5. Moreover, the control input for the proposed control strategy is realistic, and there is no switch function in FIT-SMC; therefore, the chattering issue is avoided. In a finite time, the tracking error converges to zero as presented in Fig. 6. The sliding mode enforcement is achieved at the start of the process, and the global robustness of the closed-loop system is ensured. One of the most effective ways of

TABLE 3. Performance parameters of robotic manipulator joints. The unit of all the times is secs.

Parameter	AUTAREP robotic manipulator joints			
	Waist	Shoulder	Elbow	Wrist
Settling time (t_s)	0.2060	0.2340	0.2950	0.2418
% overshoot	1.0766	1.5118	0	8.2×10^{-8}
% undershoot	0	0.1064	0.0015	0
Rise time (t_s)	0.1411	0.1567	0.2002	0.1624
Peak time (t_p)	0.2512	0.2886	5	4.9992

tackling uncertainties appears to be the SMC methodology. Sliding mode, as widely known, is precise and insensitive to disturbances [42], [43]. The joints friction torque of the robotic manipulator is estimated and trained using FFNN, as depicted in Fig. 7. However, in the dynamic model of a robotic manipulator, the friction state is not measurable; therefore, FFNN is implemented to estimate joints friction torque. Fig. 8 presents the estimated velocities of the robotic manipulator through variable-gain differentiator observer. In this methodology, it is understood that merely the measurements of position states of the robotic manipulator are accessible. The dynamics error under differentiators will con-

This article has been accepted for publication in a future issue of this journal, but has not been fully edited. Content may change prior to final publication. Citation information: DOI 10.1109/ACCESS.2021.3139041, IEEE Access

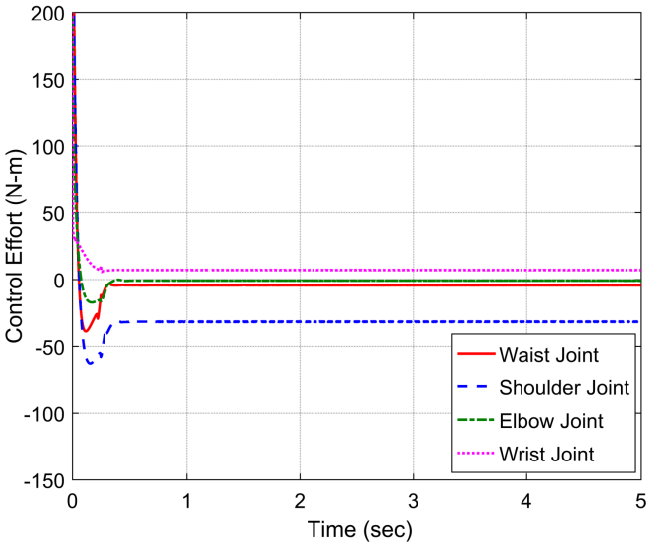

FIGURE 5. Control effort (τ_{nt}) of the robotic manipulator joints.

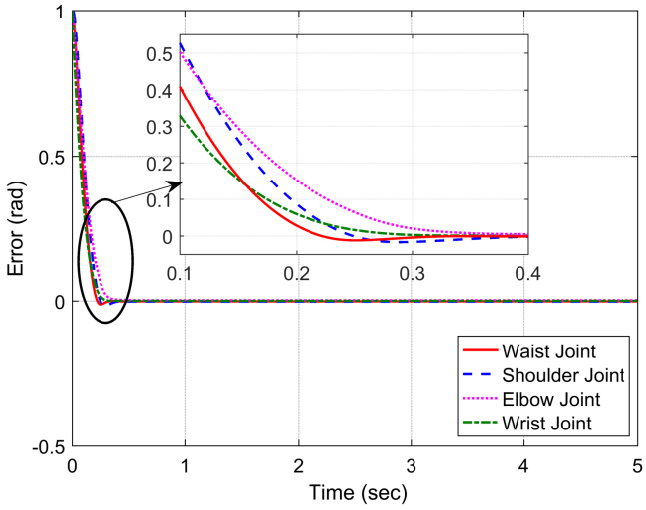

FIGURE 6. Error signals of the robotic manipulator joints.

verge to zero after the convergence procedure. It means that the estimated states reach the original states of the robotic manipulator in finite time. Fig. 9 and Fig. 10 present the step response of the waist and shoulder joints of the robotic manipulator with the RED observer and without the RED observer. The results obtained using the RED observer are compared with those when velocities of waist and shoulder joints are available for control design.

Various parameters have been identified for the performance achieved by the controller. It is important to be as accurate and comprehensive as possible; the comparative findings are summarized based on the step input signal in Table 4. This table takes into the consideration the characteristics, such as settling time, maximum percentage undershoot and overshoot, rise time, and peak time. More crucially, due to the robust behavior and excellent performance (compared to noisy information) shown by the suggested RED, the control algorithm appreciably accomplished stable tracking performance asymptotically. Hence, the newly proposed controller is chosen as the excellent candidate in the most recent control approaches because it eliminates the dependence on the corresponding sensors. Therefore, it decreases the reliance on the sensor in case of sensor failure.

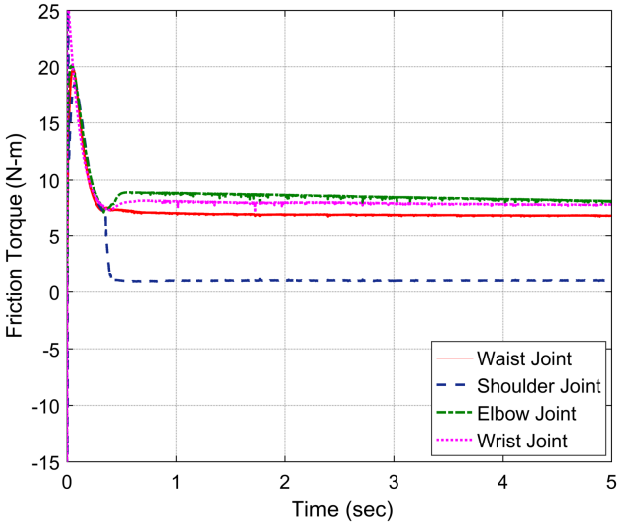

FIGURE 7. Friction torque (T_F) of the robotic manipulator joints.

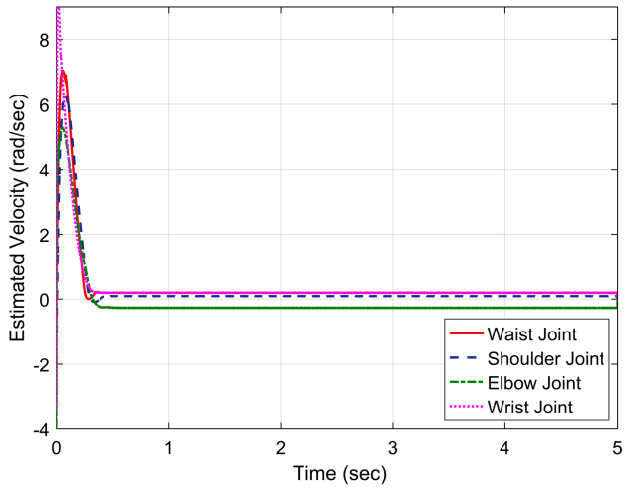

FIGURE 8. Estimated velocity of the robotic manipulator joints.

V. CONCLUSION

In this article, an AUTAREP robotic manipulator of five DoFs is, firstly, modeled using the dynamic LuGre friction model. Then, a finite-time FIT-SMC is proposed for five-DoF AUTAREP robotic manipulators, followed by a RED observer and FFNN approach. As an observer, a variable-gain RED is employed to estimate the velocity states of five-DoF AUTAREP robotic manipulator joints, which are

This article has been accepted for publication in a future issue of this journal, but has not been fully edited. Content may change prior to final publication. Citation information: DOI 10.1109/ACCESS.2021.3139041, IEEE Access

TABLE 4. Comparison of performance parameters. The unit of all the times is secs.

Parameter	AUTAREP Robotic Manipulator Joints			
	With RED		Without RED	
	Waist	Shoulder	Waist	Shoulder
Settling time (t_s)	0.2060	0.2340	0.28630	0.3640
% overshoot	1.0766	1.5118	2.5677	3.5982
% undershoot	0	0.1064	0	0.1483
Rise time (t_s)	0.1411	0.1567	0.1431	0.1574
Peak time (t_p)	0.2512	0.2886	0.2568	0.2987

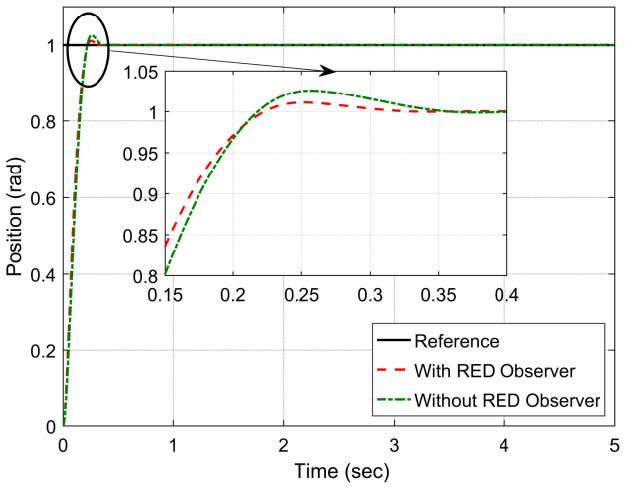

FIGURE 9. Step response of the base joint of the robotic manipulator with and without RED observer.

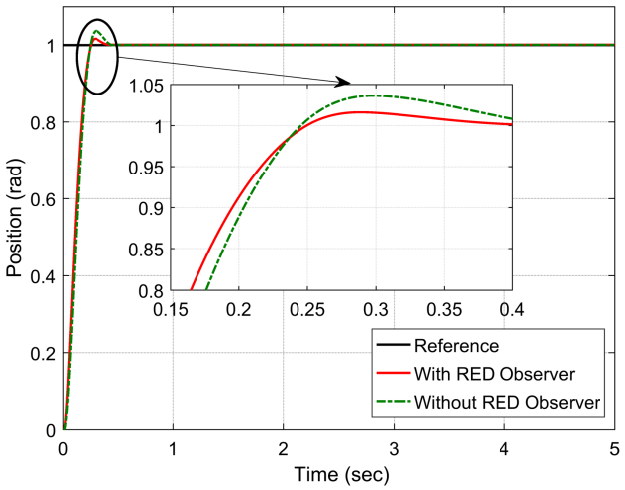

FIGURE 10. Step response of the shoulder joint of the robotic manipulator with and without RED observer.

vital for developing the suggested controller methodology. The friction is considered an unmeasurable internal state in the dynamic model of the AUTAREP robotic manipulator; therefore, FFNN is developed in which the friction torque is trained and approximated. The FIT-SMC method is employed to the AUTAREP robotic manipulator that provides finite-time convergence to the equilibrium points and guarantees good trajectory tracking performance. Furthermore, it enhanced the robust performance of the AUTAREP robotic manipulator. The proposed approaches keep the benefits of classic SMC, such as speedy response, ease of implementation, and robustness to disturbances/uncertainties, and allow the system states to reach the objective control point in a finite amount of time. The disadvantage of adopting a NN model in the proposed technique development is that it is a computationally complicated function that takes a long time to execute. It can take time for a network to converge to an optimum learning state with minimal error using conventional personal computer hardware and the backpropagation algorithm. Simultaneously, the Lyapunov candidate function is used to present the finite-time stability analysis. The simulation findings and comparison of the proposed control algorithm with RED and without RED observer validate the effectiveness of the proposed scheme.

VI. ACKNOWLEDGMENT

The authors would like to acknowledge the support of Prince Sultan University for paying the Article Processing Charges (APC) of this publication.

REFERENCES

[1] C. Garriz and R. Domingo, "Development of trajectories through the kalman algorithm and application to an industrial robot in the automotive industry," IEEE Access, vol. 7, pp. 23570–23578, 2019.
[2] S. Li, H. Wang, and M. U. Rafique, "A novel recurrent neural network for manipulator control with improved noise tolerance," IEEE transactions on neural networks and learning systems, vol. 29, no. 5, pp. 1908–1918, 2017.
[3] H.-Y. Li, I. Paranawithana, L. Yang, T. S. K. Lim, S. Foong, F. C. Ng, and U.-X. Tan, "Stable and compliant motion of physical human–robot interaction coupled with a moving environment using variable admittance and adaptive control," IEEE Robotics and Automation Letters, vol. 3, no. 3, pp. 2493–2500, 2018.
[4] S. A. Ajwad, J. Iqbal, A. A. Khan, and A. Mehmood, "Disturbance-observer-based robust control of a serial-link robotic manipulator using smc and pbc techniques," Studies in Informatics and Control, vol. 24, no. 4, pp. 401–408, 2015.
[5] G. Rigatos, P. Siano, and G. Raffo, "A nonlinear h-infinity control method for multi-dof robotic manipulators," Nonlinear Dynamics, vol. 88, no. 1, pp. 329–348, 2017.
[6] B. Dong, T. An, F. Zhou, K. Liu, and Y. Li, "Decentralized robust zero-sum neuro-optimal control for modular robot manipulators in contact with uncertain environments: theory and experimental verification," Nonlinear Dynamics, vol. 97, no. 1, pp. 503–524, 2019.
[7] Z. Dachang, D. Baolin, Z. Puchen, and C. Shouyan, "Constant force pid control for robotic manipulator based on fuzzy neural network algorithm," Complexity, vol. 2020, 2020.
[8] Y. Yanling, "Model free adaptive control for robotic manipulator trajectory tracking," The Open Automation and Control Systems Journal, vol. 7, no. 1, 2015.
[9] A. Carron, E. Arcari, M. Wermelinger, L. Hewing, M. Hutter, and M. N. Zeilinger, "Data-driven model predictive control for trajectory tracking with a robotic arm," IEEE Robotics and Automation Letters, vol. 4, no. 4, pp. 3758–3765, 2019.
[10] Y. Mehmood, J. Aslam, N. Ullah, M. Chowdhury, K. Techato, A. N. Alzaed, et al., "Adaptive robust trajectory tracking control of multiple quad-rotor uavs with parametric uncertainties and disturbances," Sensors, vol. 21, no. 7, p. 2401, 2021.

[11] N. Ullah, I. Sami, W. Shaoping, H. Mukhtar, X. Wang, M. Shahariar Chowdhury, and K. Techato, "A computationally efficient adaptive robust control scheme for a quad-rotor transporting cable-suspended payloads," Proceedings of the Institution of Mechanical Engineers, Part G: Journal of Aerospace Engineering, p. 09544100211013617, 2016.

[12] Y. Sun, J. Xu, H. Wu, G. Lin, and S. Mumtaz, "Deep learning based semi-supervised control for vertical security of maglev vehicle with guaranteed bounded airgap," IEEE Transactions on Intelligent Transportation Systems, 2021.

[13] S. Ullah, A. Mehmood, Q. Khan, S. Rehman, and J. Iqbal, "Robust integral sliding mode control design for stability enhancement of under-actuated quadcopter," International Journal of Control, Automation and Systems, vol. 18, p. 1671–1678, 2020.

[14] S.-H. Han, M. S. Tran, and D.-T. Tran, "Adaptive sliding mode control for a robotic manipulator with unknown friction and unknown control direction," Applied Sciences, vol. 11, no. 9, p. 3919, 2021.

[15] L. Zhang, J. Wang, J. Chen, K. Chen, B. Lin, and F. Xu, "Dynamic modeling for a 6-dof robot manipulator based on a centrosymmetric static friction model and whale genetic optimization algorithm," Advances in Engineering Software, vol. 135, p. 102684, 2019.

[16] F. Marques, P. Flores, J. P. Claro, and H. M. Lankarani, "Modeling and analysis of friction including rolling effects in multibody dynamics: a review," Multibody System Dynamics, vol. 45, no. 2, pp. 223–244, 2019.

[17] Y.-H. Sun, T. Chen, C. Qiong Wu, and C. Shafai, "Comparison of four friction models: feature prediction," Journal of Computational and Nonlinear Dynamics, vol. 11, no. 3, 2016.

[18] Z. A. Khan, V. Chacko, and H. Nazir, "A review of friction models in interacting joints for durability design," Friction, vol. 5, no. 1, pp. 1–22, 2017.

[19] J. Wojewoda, A. Stefański, M. Wiercigroch, and T. Kapitaniak, "Hysteretic effects of dry friction: modelling and experimental studies," Philosophical Transactions of the Royal Society A: Mathematical, Physical and Engineering Sciences, vol. 366, no. 1866, pp. 747–765, 2008.

[20] S. Wu, F. Mou, Q. Liu, and J. Cheng, "Contact dynamics and control of a space robot capturing a tumbling object," Acta Astronautica, vol. 151, pp. 532–542, 2018.

[21] J. Moreno, R. Kelly, and R. Campa, "Manipulator velocity control using friction compensation," IEE Proceedings-Control Theory and Applications, vol. 150, no. 2, pp. 119–126, 2003.

[22] F. Yue and X. Li, "Robust adaptive integral backstepping control for optoelectronic tracking system based on modified lugre friction model," ISA transactions, vol. 80, pp. 312–321, 2018.

[23] H. Saied, A. Chemori, M. El Rafei, C. Francis, and F. Pierrot, "From non-model-based to model-based control of pkms: a comparative study," in Mechanism, Machine, Robotics and Mechatronics Sciences, pp. 153–169, Springer, 2019.

[24] S. A. Al-Samarraie, "Variable structure control design for a magnetic levitation system," Journal of Engineering, vol. 24, no. 12, pp. 84–103, 2018.

[25] X. Shan and G. Cheng, "Structural error and friction compensation control of a 2 (3pus+ s) parallel manipulator," Mechanism and Machine Theory, vol. 124, pp. 92–103, 2018.

[26] J. Hu, Y. Wang, L. Liu, and Z. Xie, "High-accuracy robust adaptive motion control of a torque-controlled motor servo system with friction compensation based on neural network," Proceedings of the Institution of Mechanical Engineers, Part C: Journal of Mechanical Engineering Science, vol. 233, no. 7, pp. 2318–2328, 2019.

[27] B. Denkena, B. Bergmann, and D. Stoppel, "Reconstruction of process forces in a five-axis milling center with a lstm neural network in comparison to a model-based approach," Journal of Manufacturing and Materials Processing, vol. 4, no. 3, p. 62, 2020.

[28] B. Kim and S. Han, "Non-linear friction compensation using backstepping control and robust friction state observer with recurrent fuzzy neural networks," Proceedings of the Institution of Mechanical Engineers, Part I: Journal of Systems and Control Engineering, vol. 223, no. 7, pp. 973–988, 2009.

[29] S. Han and J. M. Lee, "Friction and uncertainty compensation of robot manipulator using optimal recurrent cerebellar model articulation controller and elasto-plastic friction observer," IET control theory & applications, vol. 5, no. 18, pp. 2120–2141, 2011.

[30] S. Grami and Y. Gharbia, "Gms friction compensation in robot manipulator," in IECON 2013-39th Annual Conference of the IEEE Industrial Electronics Society, pp. 3555–3560, IEEE, 2013.

[31] Z. Zhou and B. Wu, "Adaptive sliding mode control of manipulators based on fuzzy random vector function links for friction compensation," Optik, vol. 227, p. 166055, 2021.

[32] P. R. Ouyang, J. Tang, W. Yue, and S. Jayasinghe, "Adaptive pd plus sliding mode control for robotic manipulator," in 2016 IEEE International Conference on Advanced Intelligent Mechatronics (AIM), pp. 930–934, IEEE, 2016.

[33] V. T. Yen, W. Y. Nan, P. Van Cuong, N. X. Quynh, and V. H. Thich, "Robust adaptive sliding mode control for industrial robot manipulator using fuzzy wavelet neural networks," International Journal of Control, Automation and Systems, vol. 15, no. 6, pp. 2930–2941, 2017.

[34] Y. Sun, J. Xu, G. Lin, W. Ji, and L. Wang, "Rbf neural network-based supervisor control for maglev vehicles on an elastic track with network time-delay," IEEE Transactions on Industrial Informatics, 2020.

[35] X. Yang, S. S. Ge, and W. He, "Dynamic modelling and adaptive robust tracking control of a space robot with two-link flexible manipulators under unknown disturbances," International Journal of Control, vol. 91, no. 4, pp. 969–988, 2018.

[36] N. Shi, F. Luo, Z. Kang, L. Wang, Z. Zhao, Q. Meng, and W. Hou, "Fault-tolerant control for n-link robot manipulator via adaptive nonsingular terminal sliding mode control technology," Mathematical Problems in Engineering, vol. 2021, 2021.

[37] M. A. Arteaga, "On the properties of a dynamic model of flexible robot manipulators," 1998.

[38] N. Kapoor and J. Ohri, "Sliding mode control (smc) of robot manipulator via intelligent controllers," Journal of The Institution of Engineers (India): Series B, vol. 98, no. 1, pp. 83–98, 2017.

[39] M. W. Spong, "Seth. hutchinson, and m. vidyasagar," Robot modeling and control, 2005.

[40] L. Simoni, M. Beschi, A. Visioli, and K. J. Åström, "Inclusion of the dwell time effect in the lugre friction model," Mechatronics, vol. 66, p. 102345, 2020.

[41] C. Canudas-de Wit and R. Kelly, "Passivity analysis of a motion control for robot manipulators with dynamic friction," Asian Journal of Control, vol. 9, no. 1, pp. 30–36, 2007.

[42] S. Ullah, Q. Khan, A. Mehmood, and R. Akmeliawati, "Integral backstepping based robust integral sliding mode control of underactuated nonlinear electromechanical systems," Journal of Control Engineering and Applied Informatics, vol. 21, no. 3, pp. 42–50, 2019.

[43] S. Ullah, Q. Khan, A. Mehmood, and A. I. Bhatti, "Robust backstepping sliding mode control design for a class of underactuated electromechanical nonlinear systems," Journal of Electrical Engineering & Technology, vol. 15, pp. 1821–1828, 2020.

KHURRAM ALI is a PhD student in Electrical and Computer Engineering Department (ECE) at COMSATS University Islamabad, Pakistan. He received the BE degree in Electrical Engineering from the Air University, Pakistan, and Master of Science in Electrical Engineering from the National University of Science and Technology, Pakistan, in 2013. He has also worked as a hardware design engineer at AKSA Solution Development Services for three years. He is currently serving as a Lecturer at COMSATS University Islamabad, Pakistan. His research focus is control, automation, and robotics.

This article has been accepted for publication in a future issue of this journal, but has not been fully edited. Content may change prior to final publication. Citation information: DOI 10.1109/ACCESS.2021.3139041, IEEE Access

SAFEER ULLAH holds PhD (2021) and MS (2016) degrees in control and automation from COMSATS University Islamabad, Pakistan. He received his BS degree in Electronics Engineering from International Islamic University, Islamabad, in 2012. He is currently working as an Assistant Monitoring Officer in Khyber Pakhtunkhwa Educational Monitoring Authority. His research interests are in analysis, observation, and control of under-actuated nonlinear systems using advanced sliding mode based control approaches.

ADEEL MEHMOOD holds a PhD degree in Nonlinear Control from the Technical University of Belfort-Montbeliard, France. He earned the MS degree in robotics and embedded systems from the University of Versailles Saint-Quentin en Yvelines, France, in 2008, and BS degree in Mechatronics Engineering from the National University of Science and Technology, Pakistan, in 2006. He also worked as a Postdoctoral Researcher with the University of Haute-Alsace, France. He is currently working as an Assistant Professor at COMSATS University Islamabad, Pakistan. His research interests include robotics, renewable energy, and robust and nonlinear control of servo systems.

HALA MOSTAFA received the PhD degree in Electrical Engineering from the Faculty of Engineering and Applied Science, Memorial University, Canada, in 2014. From 2014 to 2015, she was a Research Scientist at Memorial University. She is currently an Assistant Professor at the Information Technology Department, College of Computer and Information Sciences, Princess Nourah bint Abdulrahman University, Riyadh, Saudi Arabia. Her main research interests are wireless communications, with a particular focus on smart antennas and wireless sensor networks.

MOHAMED MAREY ($SM'14$) received the MSc degree in Electrical Engineering from Menoufia University, Egypt, in 1999, and the PhD degree in Electrical Engineering from Ghent University, Belgium, in 2008. From 2009 to 2014, he was a Research Associate and a Visiting Professor with the Faculty of Engineering and Applied Science, Memorial University, Canada. He is currently a Full Professor with the Faculty of Electronic Engineering, Menoufia University, Egypt. He is on a sabbatical leave in order to join Prince Sultan University, Saudi Arabia, as a research laboratory leader of the smart systems engineering laboratory. He authored the book Multi-Carrier Receivers in the Presence of Interference: Overlay Systems (VDM Publishing House Ltd., 2009) and around 100 scientific papers published in international journals and conferences. His main research interests are wireless communications and digital signal processing, with a particular focus on smart antennas, cooperative communications, signal classification for cognitive radio systems, synchronization and channel estimation, multiple-input multiple-output antenna systems, multicarrier systems, and error correcting codes. He was a recipient of the Young Scientist Award from the International Union of Radio Science in 1999.

JAMSHED IQBAL ($SM'16$) holds a PhD in Robotics from Italian Institute of Technology (IIT) and three Master degrees in various fields of Engineering from Finland, Sweden, and Pakistan. He is currently working as a Lecturer (Assistant Professor)of Robotics in the University of Hull, UK, with more than 20 years of multi-disciplinary experience in industry and academia. He has more than 80 reputed journal papers on his credit with an H-index of 32. He is on the editorial board of several reputed journals and program committee member of various IEEE internals conferences.